Title	Effect of nanostructures orientation on electroosmotic flow in a microfluidic channel
Author(s)	Lim, An Eng; Lim, Chun Yee; Lim, Chun Yee; Taboryski, Rafael; Wang, Shu Rui
Citation	Lim, A. E., Lim, C. Y., Lam, Y. C., Taboryski, R., & Wang, S. R. (2017). Effect of nanostructures orientation on electroosmotic flow in a microfluidic channel. Nanotechnology, 28(25), 255303-.
Date	2017
URL	http://hdl.handle.net/10220/42736
Rights	© 2017 IOP Publishing Ltd. This is the author created version of a work that has been peer reviewed and accepted for publication by Nanotechnology, IOP Publishing Ltd. It incorporates referee's comments but changes resulting from the publishing process, such as copyediting, structural formatting, may not be reflected in this document. The published version is available at: [http://dx.doi.org/10.1088/1361-6528/aa734f].

Effect of nanostructures orientation on electroosmotic flow in a microfluidic channel

An Eng Lim[1], Chun Yee Lim[1], Yee Cheong Lam[1,4], Rafael Taboryski[2], and Shu Rui Wang[3]

[1] School of Mechanical and Aerospace engineering, Nanyang Technological University, 50 Nanyang Avenue, Singapore 639798
[2] Department of Micro- and Nanotechnology, Technical University of Denmark, 2800 Kongens Lyngby, Denmark
[3] Park Systems Pte Ltd, #01-07 The Alpha, Science Park 2, Singapore 117684

E-mail: myclam@ntu.edu.sg

Abstract
Electroosmotic flow (EOF) is an electric-field-induced fluid flow that has numerous micro-/nanofluidic applications, ranging from pumping to chemical and biomedical analyses. Nanoscale networks/structures are often integrated in microchannels for a broad range of applications, such as electrophoretic separation of biomolecules, high reaction efficiency catalytic microreactors, and enhancement of heat transfer and sensing. Their introduction has been known to reduce EOF. Hitherto, a proper study on the effect of nanostructures orientation on EOF in a microfluidic channel is yet to be carried out. In this investigation, we present a novel fabrication method for nanostructure designs that possess maximum orientation difference, i.e. parallel versus perpendicular indented nanolines, to examine the effect of nanostructures orientation on EOF. It consists of four phases: fabrication of silicon master, creation of mold insert via electroplating, injection molding with cyclic olefin copolymer (COC), and thermal bonding and integration of practical inlet/outlet ports. The effect of nanostructures orientation on EOF was studied experimentally by current monitoring method. The experimental results show that nanolines which are perpendicular to the microchannel reduce the EOF velocity significantly (approximately 20%). This flow velocity reduction is due to the distortion of local electric field by the perpendicular nanolines at the nanostructured surface as demonstrated by finite element simulation. In contrast, nanolines which are parallel to the microchannel have no effect on EOF, as it can be deduced that the parallel nanolines do not distort the local electric field. The outcomes of this investigation contribute to the precise control of EOF in lab-on-chip devices, and fundamental understanding of EOF in devices which utilize nanostructured surfaces for chemical and biological analyses.

Keywords: micro-/nanofabrication, deep ultraviolet lithography, reactive ion etching, injection molding, electroosmotic flow, current monitoring technique, finite element method

[4] Author to whom any correspondence should be addressed.

1. Introduction

Electroosmotic flow (EOF) is an electric-field-induced fluid flow that arises from an electrokinetic phenomenon, whereby surface charge is spontaneously formed on a solid surface upon contact with an aqueous solution. Typically, a negatively charged surface is developed when common materials such as glass or polydimethylsiloxane (PDMS) are employed for the fabrication of the micro-/nanosized channels, which attracts positive ions and repels negative ions in the electrolyte solution, resulting in a thin layer of net positive charges (nanometer thickness) known as electrical double layer (EDL). When an electric field is applied parallel to the solid surface, the positively charged EDL experiences a body force that drives its motion in the direction of the electric field. The movement of EDL is transferred to the bulk of the fluid through viscous effect, thereby generating a plug-like flow for which the EOF velocity is given by the Helmholtz-Smoluchowski slip velocity equation:

$$v_{eo} = \frac{-\varepsilon_r \varepsilon_0 E \zeta}{\mu}, \tag{1}$$

where ε_o is the permittivity of free space, ε_r is the relative permittivity of liquid, ζ is the zeta potential, E is the electric field and μ is the viscosity of fluid. This is only applicable if the EDL is thin compared to the size of the channel, which can be calculated by the Debye length (for a symmetric electrolyte):

$$\lambda_D = \sqrt{\frac{\varepsilon_0 \varepsilon_r k_b T}{2 z^2 e^2 N_A c_o}}, \tag{2}$$

where k_b is the Boltzmann constant, T is the temperature, z is the absolute charge number of the main constituent ionic species, e is the electron charge, N_A is the Avogadro constant and c_o is the concentration of electrolyte solution.

EOF has been exploited in various applications such as separation of chemical species/particles [1, 2], pumping of fluid [3, 4], mixing of analytes [5, 6], bioparticles trapping and preconcentration [7, 8]. However, EOF is not desirable in certain applications. For example, EOF generates a counterflow opposite to the electrophoresis migration of negatively charged samples, e.g. DNA and sodium dodecyl sulfate (SDS) denatured proteins, which degrades the resolution of electrophoretic separation [9]. The suppression of EOF is conventionally accomplished through the coating of water-soluble polymers [10], e.g. acidified poly(ethylene oxide) (PEO) [11]. Nanoscale networks/structures are often integrated within microchannels for a broad range of applications, such as electrophoretic separation of biomolecules [12, 13], high reaction efficiency catalytic microreactors [14, 15], and enhancement of heat transfer [16, 17] and sensing [18, 19]. Despite the investigations of EOF reduction due to nanostructured surfaces in microchannels [20-23], a proper study on the orientation effect of nanostructures is yet to be conducted.

Yasui *et al* [20] fabricated microchannels with two different types of nanopillars arrangements, i.e. the square and tilted array patterns. Both configurations had no observable EOF velocity difference between them, but both reduced EOF significantly as compared to the smooth channel. This lack of EOF velocity difference between the two configurations could well due to their insignificant orientation difference. For a rigorous investigation on the effect of nanostructures orientation on EOF, the nanostructure designs in microchannels should demonstrate a significant orientation difference. To maximize the orientation difference, a novel method for the fabrication of

microchannels with arrays of parallel and perpendicular indented nanolines is developed. The micro- and nanostructures produced are of good regularity, cover a relatively large area and can be mass-produced. Despite the availability of various micro-/nanofabrication techniques, most of them do not satisfy the aforementioned criteria.

Traditional methods to produce micro-/nanostructured devices include micro-electro-mechanical system (MEMS) fabrication technologies [12, 24] and rapid prototyping techniques, such as micromilling [25, 26], laser micromachining [27, 28] and PDMS soft lithography [29, 30]. Although these methods are well-established with their own advantages, they suffer from certain drawbacks. The main benefits of micromilling and laser micromachining are the high repeatability, flexibility and cost efficiency [31, 32], but their resolutions are limited at micrometer level. Although PDMS soft lithography is popular for its low material costs, fast prototyping and optical transparency [33, 34], the filling of high viscosity PDMS into nanoscale features on the master mold remains a challenge [35-37]. MEMS technologies, such as lithography and wet/dry etching, allow the fabrication of nanoscale patterns along with microscale structures on silicon (Si) or glass platform [38, 39], but the complexity of the process lowers the throughput and increases the cost, especially for single-use microfluidic devices.

Ideally, the manufacturing of micro-/nanostructured devices for practical research and applications should fulfill the following requirements: (i) ease of mass production, (ii) low material costs, (iii) high flexibility, (iv) high replication accuracy and (v) good controllability of micro-/nanoscale patterns. Polymer-based replication methods, such as hot embossing (subset of nanoimprint lithography (NIL)) [40-42] and injection molding [43-45], are compatible with the requirements of low material costs and high replication accuracy. Among these methods, injection molding is more suitable for mass production due to the short cycle times. However, conventional injection molding tools are expensive and time consuming to fabricate. Furthermore, the machining of the molding tools is challenging for nanoscale features. To overcome these shortcomings, MEMS technologies can be employed for the fabrication of masters for injection molding.

Many cleanroom-based techniques have been reported for the creation of mold insert [46, 47]. The most commonly used technique is LIGA (**LI**thographie, **G**alvanoformung, **A**bformung, which means Lithography, Electroplating, Molding in German) [48, 49]. This technique may be categorized into two main types, namely X-ray LIGA and UV LIGA, that utilize highly collimated synchrotron X-rays and ultraviolet light respectively. Although X-ray LIGA enables the production of high aspect ratio structures, the process is complicated and requires an expensive synchrotron facility. In contrast, UV LIGA is cheaper and more accessible due to the use of inexpensive UV light source and less sophisticated chromium mask, but it creates relatively low aspect ratio structures. Despite the employment of versatile polymer photoresist, LIGA faces technical difficulties when multilevel structuring and nano-range precision molds are needed. DEEMO (**D**ry **E**tching, **E**lectroplating, **MO**lding) [50] substitutes the X-ray lithography step of LIGA with dry etching, which makes it possible to produce structures of feature sizes from nanometers to micrometers. However, multilevel structuring involving both micro- and nanoscale still remains a challenge for DEEMO, as the dry etching process might destroy the regularity of nanoscale patterns.

In this investigation, a novel fabrication process is developed, namely a hybrid LIGA-DEEMO process for the fabrication of microchannels with large-area arrays of parallel and perpendicular indented

nanolines. These two fundamentally different technologies were combined to exploit the strengths of both methodologies. To ensure good regularity and controllability over the nanoscale patterns, deep UV (DUV) lithography [51, 52] was adopted instead of the conventional electron beam lithography (EBL) [53, 54], as EBL is costly and time consuming for large-area structuring. This process allows the fabrication of nanostructures having significant orientation difference, namely parallel and perpendicular indented nanolines. Both types of structures were fabricated via injection molding of cyclic olefin copolymer (COC) and sealed by thermal bonding. The orientation effect of nanostructures (parallel versus perpendicular indented nanolines) on EOF in a microfluidic channel was examined experimentally by current monitoring technique, and numerically by finite element simulations.

2. Fabrication methods

2.1. Microchannel design with different nanostructured surfaces

Figure 1(a) shows the exploded view of the entire micro-/nanofluidic device. The injection molded COC chip has dimensions of 75 mm x 25 mm x 1 mm, which is similar to that of a standard microscope slide. The molded chip was sealed via thermal bonding with a thin COC foil (thickness of approximately 100 µm) to provide enclosure for the open microchannel, as well as address the requirement of short working distance for high magnification microscopy experiments. Practical inlet/outlet ports were also integrated to the system through the use of female luer lock couplers for easy fluidic access.

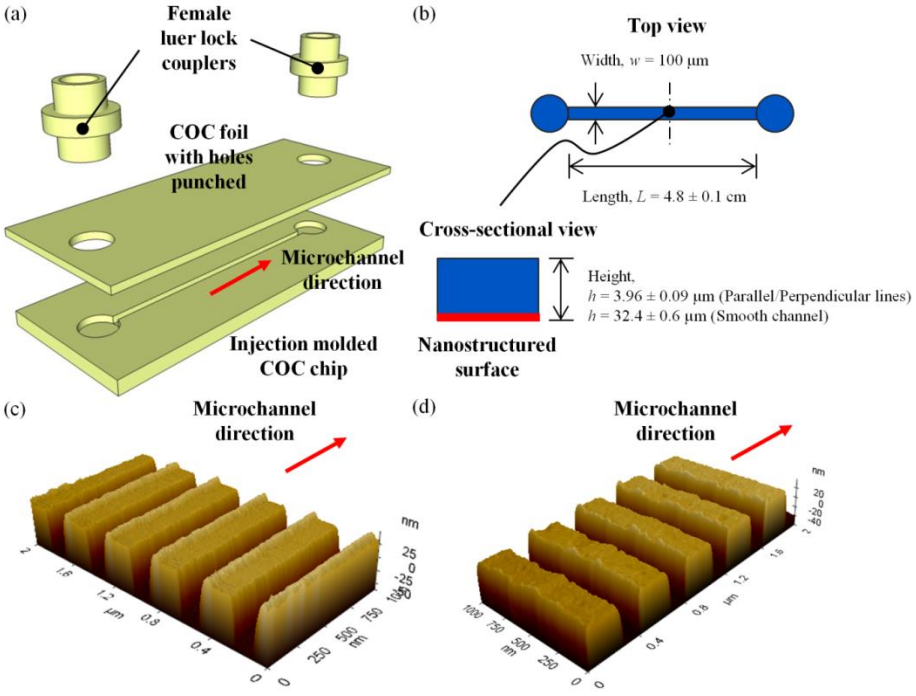

Figure 1. (a) Exploded view of micro-/nanofluidic device. (b) Schematic diagram of microchannels with different nanostructured surfaces (not drawn to scale). Atomic force microscope (AFM) images of (c) parallel and (d) perpendicular indented nanolines on the bottom walls of the respective microchannels.

Design of the microchannels with different nanostructures is represented by the schematic diagram as shown in figure 1(b). The rectangular microchannel has width of 100 μm and length of 4.8 ± 0.1 cm, with large-area arrays of parallel/perpendicular indented nanolines (period of 397.6 ± 4.3 nm, line width of 184.6 ± 10.7 nm and depth of 93.4 ± 8.5 nm) on the bottom wall of the channel. Characterizations of the parallel and perpendicular indented nanolines inside the respective microchannels were performed with the aid of an atomic force microscope (AFM, Park NX20). Figure 1(c) to 1(d) show the AFM images of the different nanostructured surfaces. A smooth microchannel without any nanostructure (roughness arithmetic mean value *Ra* = 5.5 ± 0.6 nm) was also fabricated via the conventional DEEMO process (refer to Supplementary Data for more details) to serve as a comparison to the microchannels with nanostructures. The heights of the microchannels with parallel/perpendicular indented nanolines are 3.96 ± 0.09 μm, and the height of the smooth microchannel is 32.4 ± 0.6 μm, as measured by a Dektak-XT stylus surface profiler. The smooth channel serves as a benchmark for the measurement of zeta potential and EOF velocity without nanostructured surface. The additional channel height allows ease of fabrication but does not affect the flow velocity as EOF generates the same flow velocity regardless of cross section area [55, 56].

2.2. Hybrid LIGA-DEEMO process for the fabrication of master structures on silicon wafers

Fabrication of Si masters for microchannels with large-area arrays of parallel and perpendicular indented nanolines involves a two-step lithography process (see figure 2): (i) DUV lithography for the production of nanolines and (ii) standard UV lithography for the construction of microchannel. The DUV lithography process started with hexamethyldisilazane (HMDS) deposition on the silicon wafers to remove native oxide. This is followed by spin coating of bottom anti-reflective coating (BARC) (DUV42P, Nissan Chemical) and then 350 nm thick positive resist (M230Y, JSR Micro). Subsequently, the wafers were prebaked at 90 °C for 130 s. Four exposures were performed using Canon FPA-3000 EX4 stepper (KrF laser as light source, wavelength of 248 nm) with dose of 24 mJ/cm^2 to stitch (accuracy of 3σ (standard deviations) = 35 nm) the parallel/perpendicular line grating (period of 400 nm, line width of 200 nm and grating area of 100 μm x 1.25 cm) to form the bottom surface of the microchannel (base area of 100 μm x 5cm). After the exposures and post baking at 130 °C for 1 min, the wafers were puddled in the developer (MF CD-26 developer, Rohm and Haas Electronic Materials LLC) for 1 min. To reveal the Si surface, BARC layer in the developed structures was removed by pure oxygen plasma. The wafers were then exposed to C_4F_8/SF_6 plasma (75/38 sccm) reactive ion etching (RIE) in STS Pegasus system (coil/platen power = 800/40 W, pressure = 4 mtorr, temperature = -20 °C and t = 110 s.). Thereafter, the remaining DUV resist and BARC were stripped in TePla 300 plasma asher for 10 min with flow rate of O_2 at 400 sscm, N_2 at 70 sscm, pressure of 1 mbar and power of 1000 W. The etched parallel and perpendicular nanolines have period of 399.8 ± 5.3 nm, line width of 176.2 ± 4.1 nm and depth of 94.0 ± 3.8 nm, as characterized by Park NX20 AFM.

A second lithography step (standard UV lithography process) was performed for the construction of the microchannel. The etched Si wafers were vacuum baked at 90 °C for 5 min, followed by HMDS priming for 5 min (YES-310TA-E vapor prime oven, Yield Engineering System) to promote adhesion of the photoresist. A 4.2 μm thick layer of positive resist (AZ 5214E, MicroChemicals) was spin coated on the wafers using a SSE Maximus 804 cluster system. The spin speed was first set at 725 rpm for 1 min, followed by 3500 rpm for 10 s. Subsequently, prebaking was conducted at 95 °C for 90 s in 1 mm proximity. A chrome mask was used to define the flow channel pattern (width of 100 μm and length of 5

cm). The desired microchannel pattern was aligned with the etched parallel/perpendicular nanolines through the alignment marks (created during DUV process), and transferred onto the wafers using Karl Süss MA6/BA6 contact aligner (350 W Hg lamp with i-line filter as light source, exposure wavelength of 365 nm) in hard contact mode with exposure dose of 140 mJ/cm^2. After that, the exposed wafers were immersed in developer (AZ 351B, MicroChemicals) for 1 min. The developed microchannels have width of 100 µm and height of 4.2 µm, as measured by Dektak-XT stylus profiler.

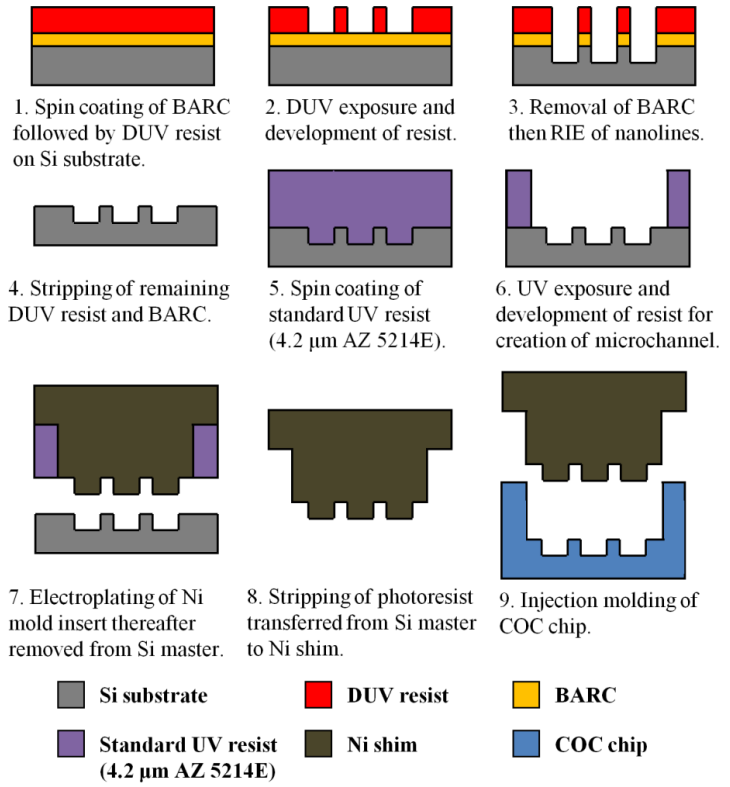

Figure 2. Schematics of hybrid LIGA-DEEMO fabrication process for microchannels with large-area arrays of parallel and perpendicular indented nanolines.

2.3. Creation of mold inserts via electroplating

To carry out injection molding, a metal mold insert is fabricated because silicon is too brittle for the injection molding process. Hence, negative mold inserts were fabricated by electroplating nickel (Ni) onto the Si wafers produced previously (refer to section 2.2). Mold inserts produced in this manner can withstand several thousand cycles, which are ideally suited for mass production settings. For electroplating to proceed, the surface being deposited on must be conductive. As such, a seed layer of approximately 85 nm nickel/vanadium (Ni/V, 93/7 wt%) was sputtered onto the Si wafers (Custom system, Kurt J. Lesker). The vanadium serves to inhibit oxidation of nickel, which would otherwise interfere with the electroplating process. Then, the sputtered wafers were left in the nickel bath (Microform 200, Technotrans) for approximately 6 h to electroplate shims of 350 µm thickness (maximum current of 3.5 A and charge of 18.1 Ah). The Ni shims were loosely attached to the Si masters, and thus they can be easily removed from the wafers. Resist transferred from the Si masters to the Ni shims were stripped in TePla 300 plasma asher for 20 min with flow rate of O_2 at 400 sscm, N_2 at 70

sscm, pressure of 1 mbar and power of 1000 W. Before the injection molding process, the negative Ni mold inserts were coated with perfluorodecyltrichlorosilane (FDTS) monolayer (MVD100E, Applied Microstructures) to function as anti-stiction layer.

2.4. Injection molding with cyclic olefin copolymer

Replicas of the master structures were injection molded in an Engel Victory 80/45 Tech hydraulic injection molder equipped with an Engel ERC 13/1-F pick up robot. The negative Ni mold inserts were fitted into the molding tool of the machine, which is custom designed to produce polymer chips with the dimensions of a standard microscope slide (refer to section 2.1). Parts were injection molded in TOPAS 5013L-10 COC from Topas Advanced Polymers GmbH. Due to the relatively high glass transition temperature of 135 °C, TOPAS 5013L-10 COC is well-suited for experiments at elevated temperatures, e.g. melting of double-stranded DNA for separation into two single strands (also known as DNA denaturation) [57] and polymerase chain reaction (PCR) amplification of DNA in COC microfluidic devices [58]. Furthermore, it has high flowability that should facilitate the filling of nanoscale cavities on the mold inserts. A variotherm process was employed for the injection molding, with melt temperature of 270 °C, mold temperature of 130 °C, injection pressure of 950 bar, injection speed of 40 mm/s, holding pressure of 400 bar for 10 s and demolding temperature of 95 °C, which resulted in a overall cycle time of about 2 to 4 min. High replication quality of the molded micro- and nanostructures was observed from the characterizations of injection molded COC chips and Si masters through the use of Dektak-XT stylus profiler and Park NX20 AFM (refer to section 2.1 and 2.2).

2.5. Thermal bonding and integration of practical inlet/outlet ports

The injection molded chips were sealed to 101.6 μm thick extruded TOPAS COC foils of the same grade by thermal bonding (Specac Atlas manual hydraulic press with heated platens). Entrance and exit holes were punched on the COC foil (approximately 5 cm apart), and aligned with the open microchannel on the molded chip (see figure 1(a)). To ensure uniform pressure across the chip surface, the molded chip and the foil were sandwiched between two thin PDMS layers (approximately 3 mm thick for each layer) for compensating slight non-uniformities in flatness. A piston force of 0.25 kN was applied for 10 min with temperature of 128 °C to bond the chip to the foil.

Practical inlet and outlet ports were integrated to the devices via the use of white nylon female luer lock couplers (Cole-Parmer) to connect the microchannels to external flow or air pressure control (see figure 1(a)). UV adhesive, Dymax 215-CTH-LV-UR-SC exhibits excellent adhesion between the nylon coupler and COC chip. However, the UV adhesive often flows and clogs the inlet and outlet of the microchannel when it is applied directly to the chip due to its low viscosity. To overcome this, the luer lock couplers were first attached to the inlet and outlet with Pro-Spec epoxy steel adhesive (mixing ratio 1:1 and set time of 4 min), which restricts the flow of the UV adhesive into the microchannel. An UV flood curing system (UVF600, Technodigm) was employed to cure the UV adhesive for 8 min. The blue color of the UV adhesive turns colorless when it is fully cured. Subsequently, the device was left under normal room conditions for 24 h so that the adhesive can reach its full strength.

3. Experimental details

3.1. Current monitoring experiment

Current monitoring experiments [59-62] (see figure 3(a)) were conducted to investigate the orientation effect of nanostructures (parallel versus perpendicular indented nanolines) in microchannel on EOF. EOF of two fluids with dissimilar ionic species [63, 64] or large concentration difference [65, 66] induces pH change and exhibits hysteretic behavior, whereby the flow rate/velocity is directional-dependent, i.e. the flow rate/velocity for fluid A displacing fluid B is different from fluid B displacing fluid A. Furthermore, electrolysis at the electrodes generates hydronium (H_3O^+) and hydroxide (OH^-) ions will alter the pH in the reservoirs [67]. Several precautions have been implemented in the experiments to ensure negligible pH change in the reservoirs. Sodium bicarbonate ($NaHCO_3$) buffered solution (Sigma-Aldrich) was employed to keep the pH constant throughout the experiments. Large-volume reservoirs (200 µL) were used to significantly dilute the concentrations of H_3O^+ and OH^- ions produced at the electrodes from electrolysis. The large reservoirs also ensure negligible liquid level change, thereby minimizing the back pressure generated [68]. The short experimental time (less than 2 min) and small electric current (0.0392-1.57 µA) as a result of the small microchannel cross section (400/3200 μm^2) and low conductivity solution, limit the production of H_3O^+ and OH^- [69]. pH indicator strips (Merck 109535) were employed to measure the pH of the solution in the reservoirs before and after the experiments. The pH change was found to be negligible.

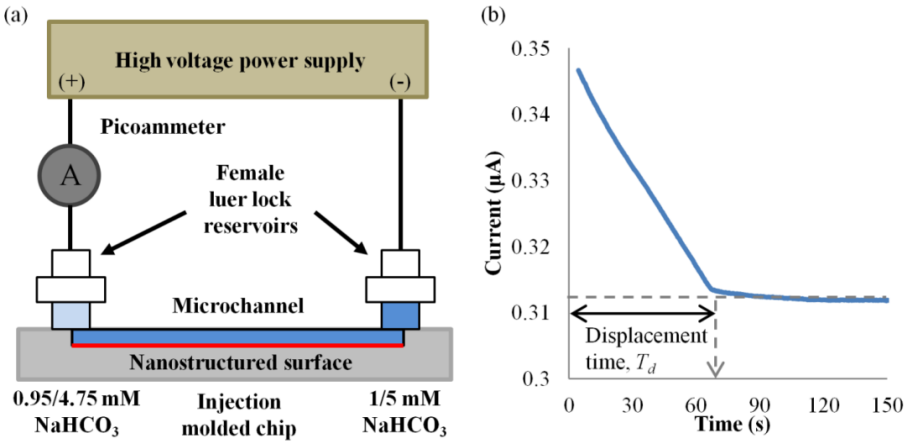

Figure 3. (a) Schematic diagram of experimental setup for current monitoring method. (b) Current-time curve for EOF displacement of 1 mM $NaHCO_3$ with 0.95 mM $NaHCO_3$ in smooth microchannel.

0.95 mM, 1 mM, 4.75 mM and 5 mM concentrations of $NaHCO_3$ were prepared. The measured conductivities (IONCheck 65, Radiometer Analytical) for the solutions are 88.4 ± 0.2 µS/cm, 93.8 ± 0.3 µS/cm, 437.4 ± 0.5 µS/cm and 466.6 ± 0.2 µS/cm respectively. The measured pH (FEP20, Mettler Toledo) for the solutions are 7.74 ± 0.02, 7.90 ± 0.02, 8.41 ± 0.01 and 8.69 ± 0.01 respectively. The microchannels were flushed with $NaHCO_3$ for 10 min through the inlet port at 20 psi (100DM Syringe Pump, Teledyne Isco), with the outlet port exposed to the atmosphere. Thereafter, white nylon male luer plug (Cole-Parmer) was secured on the outlet port to stop the flow, and to maintain a constant pressure of 20 psi in the microchannel for another 10 min. This is to facilitate the filling of the nanostructures. In addition, the microchannels were flushed with $NaHCO_3$ by EOF for 15 min, to ensure that the nanostructures are completely filled. The microchannel and reservoir connecting to the cathode were filled with 1/5 mM $NaHCO_3$, while reservoir connecting to the anode was filled with 0.95/4.75 mM $NaHCO_3$ (95% of residing solution) (see figure 3(a)). Electric potential of 500 V (CZE1000R, Spellman)

was applied across the reservoirs to induce EOF. The resultant current change was monitored by a picoammeter (Keithley 6458) in series to the channel. The time for the current to reach a steady value, i.e. displacement time, was determined from the current-time curve (see figure 3(b)). The average EOF velocity can subsequently be determined by dividing the length of channel with the displacement time:

$$v_{avg} = \frac{L}{t_d}, \tag{3}$$

where L is the length of microchannel and t_d is the displacement time.

Effect of Joule heating, which causes EOF to deviate from its normal plug-like velocity flow profile, is insignificant as the conductivities of the solutions employed were low [70]. A conservative estimate of Joule heating can be calculated from the energy balance between energy generation E_g and energy storage ΔE_{st} in the liquid [71]. For the chosen experimental parameters, the worst case scenario has an estimated temperature rise of 0.7 °C, which is negligible.

3.2. Numerical simulation

Numerical simulations were conducted on steady-state EOF for 1 mM $NaHCO_3$ through finite element method (FEM). The simulations were based on Poisson-Nernst-Planck (PNP) model with modified boundary conditions [63-65]. The simulations were implemented on COMSOL Multiphysics software. 2-D simulations were performed to investigate the effect of perpendicular indented nanolines on EOF in the microchannel, in comparison to a smooth microchannel. The simulation domains and boundary conditions are shown in figure 4. The simulation model was meshed with triangular elements. The size of the elements at the wall boundaries was set to 1-2.5 nm, and the size of each adjacent element further from the wall increased by 1.05 times. The applied potential, electrostatic potential and ion concentrations were discretized with second order elements, while the pressure and velocity were discretized with linear elements. Convergence test was performed with higher number of elements and the numerical error is found to be negligible for this mesh selection. The convergence criterion was based on relative tolerance of less than 0.001 between subsequent iterations.

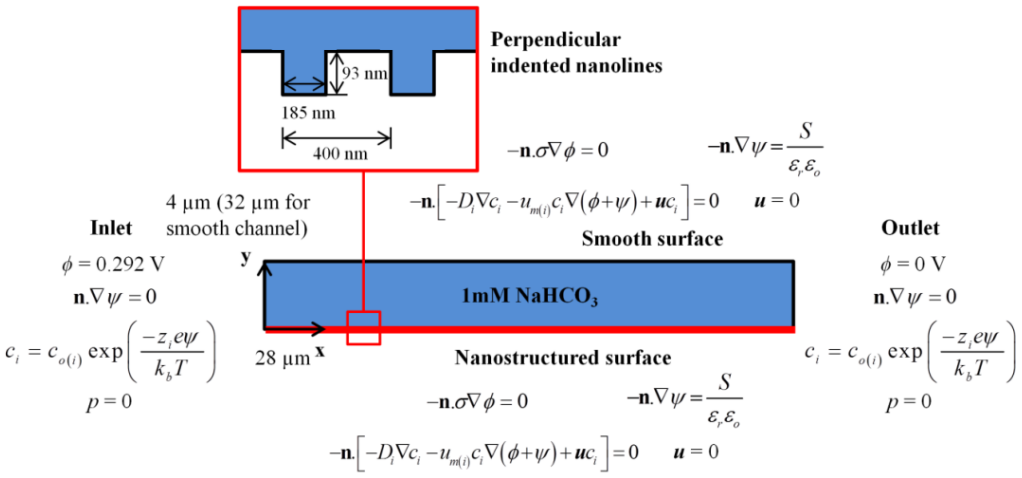

Figure 4. Numerical simulation domains and boundary conditions.

The numerical simulations were performed by solving the Laplace equation (equation 4), Poisson equation (equation 5) and Nernst-Planck equation (equation 6) simultaneously with the Navier-Stokes and continuity equations (equations 7 and 8) to obtain the fluid flow field. The governing equations are:

$$\nabla.\left(\sigma\nabla\phi\right)=0\,, \tag{4}$$

$$\nabla.\nabla\psi=-\frac{\rho_e}{\varepsilon_r\varepsilon_o}\,, \tag{5}$$

$$\frac{\partial c_i}{\partial t}+\nabla.\left[-D_i\nabla c_i-u_{m(i)}c_i\nabla\left(\phi+\psi\right)\right]=-\boldsymbol{u}.\nabla c_i\,, \tag{6}$$

$$\rho\frac{\partial\boldsymbol{u}}{\partial t}=-\nabla p+\mu\nabla^2\boldsymbol{u}+\rho_e\left[-\nabla\phi\right], \tag{7}$$

$$\nabla.\boldsymbol{u}=0\,, \tag{8}$$

where ϕ is the applied electric field, $\sigma = F\sum z_i u_{m(i)} c_i$ is the solution conductivity, F is the Faraday constant, z_i is the charge number, c_i is the concentration, D_i is the diffusion coefficient, $u_{m(i)}$ is the ionic mobility of ionic species, ψ is the wall electrostatic potential, $\rho_e = F\sum c_i z_i$ is the net charge density, $\boldsymbol{u}$ is the fluid velocity, ρ is the fluid density and p is the pressure. The symbols and values of parameters used in the numerical simulations are given in table 1.

Table 1. Symbols and values of parameters employed in numerical simulations. Ionic mobility of a ion species is calculated through the formula $(z_i D_i F)/(RT)$.

Parameters	Symbol (Unit)	Value
Permittivity of free space	ε_o ($C.V^{-1}.m^{-1}$)	8.85×10^{-12}
Relative permittivity	ε_r	80
Viscosity of water	μ ($kg.m^{-1}.s^{-1}$)	8.90×10^{-4}
Density of water	ρ ($kg.m^{-3}$)	1000
Faraday constant	F ($C.mol^{-1}$)	96485
Gas constant	R ($J.mol^{-1}.K^{-1}$)	8.314
Boltzmann constant	k_b ($m^2.kg.s^{-2}.K^{-1}$)	1.381×10^{-23}
Temperature	T (K)	298
Electron charge	e (C)	1.602×10^{-19}
Avogadro constant	N_a (mol^{-1})	6.022×10^{23}
Solution concentration	c_o ($mol.m^{-3}$)	1
Surface charge density	S ($C.m^{-2}$)	-9.86×10^{-3}
Diffusion coefficient of Na^+	D_{Na^+} ($m^2.s^{-1}$)	1.334×10^{-9}
Diffusion coefficient of HCO_3^-	D_{HCO3^-} ($m^2.s^{-1}$)	1.105×10^{-9}

Ionic mobility of Na^+	$u_{m(Na^+)}$ ($m^2.V^{-1}.s^{-1}$)	5.194×10^{-8}
Ionic mobility of HCO_3^-	$u_{m(HCO3^-)}$ ($m^2.V^{-1}.s^{-1}$)	-7.919×10^{-8}
Ionic charge number of Na^+	z_{Na^+}	+1
Ionic charge number of HCO_3^-	z_{HCO3^-}	-1

4. Results and discussion

The displacement times of 1 mM $NaHCO_3$ in microchannels with large-area arrays of parallel and perpendicular indented nanolines were measured with current monitoring method, in comparison to a smooth microchannel (see figure 5(a)). The measured displacement times of 1mM $NaHCO_3$ for microchannels with parallel and perpendicular indented nanolines are 66.5 ± 3.6 s and 83.5 ± 9.0 s respectively, and for smooth microchannel is 66.7 ± 2.7 s.

The experiments were repeated for 5 mM $NaHCO_3$. Increasing the concentration of $NaHCO_3$ by 5 times decreases the Debye length from approximately 10 nm to 4 nm respectively for 1 mM and 5 mM $NaHCO_3$ (as calculated by equation 2). The measured displacement times of 5 mM $NaHCO_3$ for microchannels with parallel and perpendicular indented nanolines are 73.5 ± 4.4 s and 93.8 ± 6.7 s respectively, and for smooth microchannel is 73.2 ± 2.5 s. The experimental results for 5 mM $NaHCO_3$ (see figure 5(a)) shows a similar trend in flow rate reduction as observed for 1 mM $NaHCO_3$.

For microchannel with perpendicular indented nanolines, the displacement time is increased by approximately 25%. According to equation 3, the result reveals that EOF velocity is lowered by the introduction of nanostructured surface in the microchannel. This observation agrees with the existing literatures [20-23] which suggest that nanostructured surface significantly reduces EOF. However, negligible difference in the flow velocity is observed for the microchannel with parallel indented nanolines.

For pressure driven flow, the fluid flow velocity is determined by the hydraulic resistance which is inversely proportional to the cross sectional area of the channel. A channel with larger cross section yields a low hydraulic resistance and thus a higher flow velocity. However, this concept is not applicable to EOF. EOF produces the same flow velocity regardless of cross section area [55, 56]. Therefore, the difference in cross sectional area for smooth microchannel and microchannel with perpendicular nanolines is not the cause for the observed flow velocity difference.

EOF velocity is dependent on the electric field, permittivity and viscosity of the liquid, and the zeta potential developed at the channel wall (as indicated by equation 1). Zeta potential, a measure of the surface properties, is an important parameter that dictates the direction and velocity of EOF. The nominal "material" zeta potential is the same in both smooth and nanostructured microchannels since they are fabricated from the same material. The "effective" zeta potential concept is proposed here to encompass both the effect of nanostructures and the zeta potential of the virgin material to describe the EOF discrepancy between the smooth and nanostructured channels.

Since the thickness of EDL is thin compared to the micro-/nanostructures of the injection molded COC chips (refer to section 2.1), the effective zeta potential which includes the chemical properties and

the topography of the surface can be derived by substituting the average EOF velocity from equation 3 into equation 1, and expressed as:

$$\zeta_{eff} = \frac{-\mu}{\varepsilon_r \varepsilon_0 E} \cdot \frac{L}{t_d} . \tag{9}$$

The introduction of an effective zeta potential exemplifies the strong correlation between the EOF velocity and the surface topography. Magnitude of effective zeta potentials of 1 mM and 5 mM $NaHCO_3$ in microchannels with parallel and perpendicular indented nanolines are shown in figure 5(b), as compared to the smooth microchannel. The effective zeta potentials of 1 mM $NaHCO_3$ for microchannels with parallel and perpendicular indented nanolines are 87.3 ± 4.5 mV and 70.1 ± 7.8 mV respectively, and for smooth microchannel is 87.0 ± 3.5 mV. The effective zeta potentials of 5 mM $NaHCO_3$ for microchannels with parallel and perpendicular indented nanolines are 79.0 ± 4.9 mV and 62.0 ± 4.5 mV respectively, and for smooth microchannel is 79.2 ± 2.9 mV. It can be observed that the magnitude of effective zeta potential (and thus EOF velocity) is reduced significantly (approximately 20%) for microchannel with perpendicular indented nanolines. In contrast, there is negligible difference in effective zeta potential between the smooth microchannel and the microchannel with parallel indented nanolines.

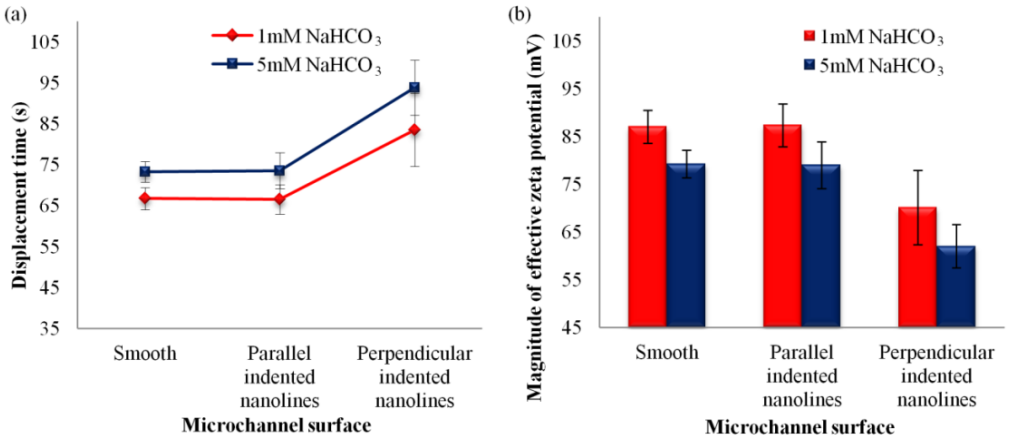

Figure 5. (a) Displacement times and (b) magnitude of effective zeta potentials for microchannels with large-area arrays of parallel and perpendicular indented nanolines, in comparison to smooth microchannel, for 1 mM and 5 mM $NaHCO_3$.

Our investigation demonstrates for the first time that *the orientation of nanostructures*, and not just the presence of nanostructures, is an important factor which affects EOF behavior. EOF originates from the interaction between the EDL and the applied electric field. The nanostructures distort the local electric field at the wall, and thus affect the effective zeta potential and the flow velocity. For the microchannel with parallel nanolines, it can be deduced that the electric field is not distorted by the parallel nanolines as they are in the same direction as the electric field. Thus, the flow velocity is the same as the smooth microchannel, which agrees with the experimental observations. For the microchannel with perpendicular nanolines, finite element simulation indicates that the perpendicular nanolines distort the electric field which follows the contour of the nanostructures (see figure 6(a)), and reduce the average electric field along the surface from 104 V/cm to 73.3 V/cm. This reduces the fluid flow velocity across the entire microchannel as electroosmotic flow is driven by the electric field at the surface (see figure

6(b)). The simulation predicts that the average fluid velocity for 1 mM $NaHCO_3$ is decreased from 7.23 x 10^{-4} m/s to 6.33 x 10^{-4} m/s. This prediction agrees well with the observed velocity reduction of (7.21 ± 0.29) x 10^{-4} m/s to (5.81 ± 0.65) x 10^{-4} m/s in the experiments.

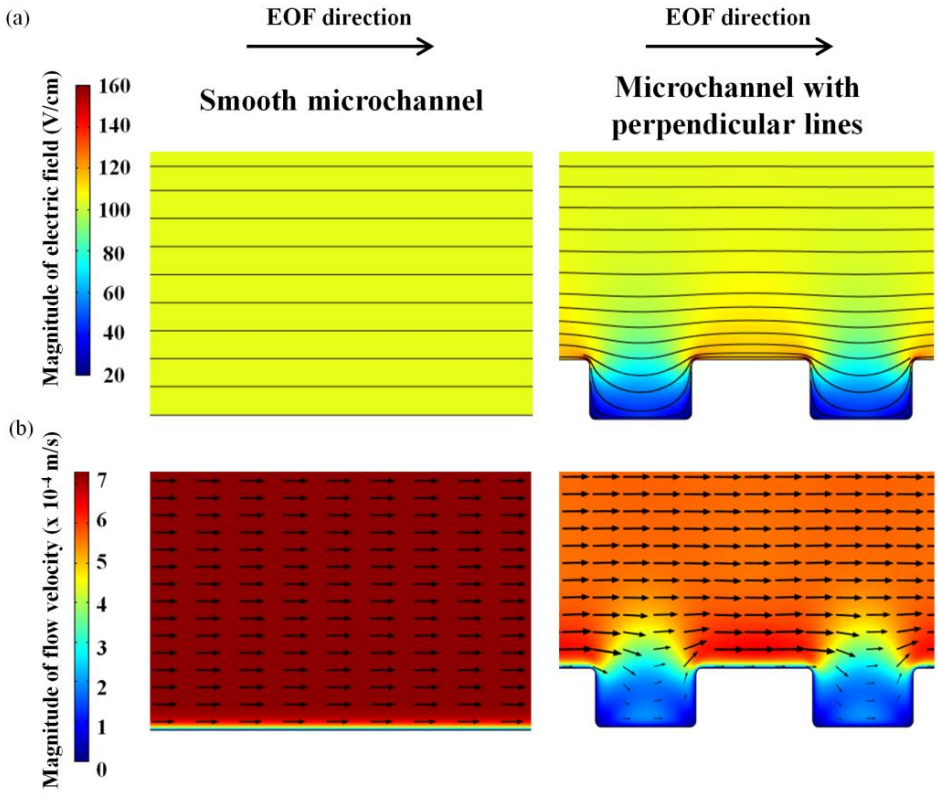

Figure 6. Simulated (a) electric field lines and (b) fluid flow velocity profile for smooth microchannel, and microchannel with perpendicular indented nanolines, for 1 mM $NaHCO_3$.

The orientation of the nanostructures dictate the distortion of the local electric field, and thus the effective zeta potential. Yasui *et al* [20] fabricated microchannels with two different types of nanopillars arrangements, i.e. the square and tilted array patterns. Both nanopillar configurations had no observable EOF velocity difference between them, but both reduced EOF significantly as compared to a smooth channel. This lack of EOF velocity difference between the two configurations could well due to their insignificant orientation difference. However, nanolines are significantly different from nanopillars because the arrangement of nanolines determines the degree of EOF suppression. We have demonstrated the two extremes, the perpendicular nanolines distort the electric field significantly, and in contrast the parallel nanolines do not distort the electric field at all. As such, the parallel nanolines do not affect EOF, while the perpendicular nanolines reduce EOF significantly.

5. Conclusion

In this investigation, we presented a fabrication method for nanostructure designs in microchannels that possess maximum orientation difference, i.e. parallel versus perpendicular indented nanolines, to examine the orientation effect of nanostructures on EOF. The fabrication process can be divided into four phases: fabrication of master structures on Si wafers, creation of mold inserts via

electroplating, injection molding with COC, and thermal bonding and integration of practical inlet/outlet ports. The novel feature of this fabrication method is the demonstration of hybrid LIGA-DEEMO process for the fabrication of microchannels with large-area arrays of parallel and perpendicular indented nanolines, which exploits the strengths of these two fundamentally different technologies to ensure good regularity and controllability over the nanoscale patterns.

This fabrication method allows the fabrication of nanostructures with significant orientation difference. This facilitates the investigation of the orientation effect of nanostructures on EOF by the current monitoring technique. The "effective" zeta potential concept is proposed here to encompass both the effect of nanostructures and the zeta potential of the virgin material to describe the EOF discrepancy between the smooth and nanostructured channels. The experimental results show a significant reduction in the effective zeta potential (and thus EOF velocity) with the introduction of perpendicular indented nanolines in a microchannel. In contrast, negligible difference was observed on effective zeta potential between a smooth microchannel and a microchannel with parallel indented nanolines. EOF originates from the interaction between EDL and the applied electric field. The nanostructures distort the local electric field at the wall as shown by the numerical results, with the distortion of the electric field a function of nanostructures orientation. Thus, the nanostructures orientation has a direct bearing on the effective zeta potential and flow velocity. The outcomes of this investigation will enhance the fundamental understanding of EOF behavior and have implications on the precise EOF control in devices utilizing nanostructured surfaces for chemical and biological analyses.

Acknowledgments

The authors would like to gratefully acknowledge Agency for Science, Technology and Research (A*STAR) for its financial support (SERC grant no. 122-PSF-0019). An Eng Lim thanks Technical University of Denmark (DTU Nanotech) for hosting his research attachment, and also Danchip for assistance with the fabrication of the micro-/nanofluidic devices. Special thanks to Tian Kooi Chin, Park Systems Pte Ltd, for facilitating the characterization of the devices with Park NX20 AFM. Lastly, An Eng Lim thanks Nanyang Technological University (NTU) for awarding him a Ph.D. scholarship.

References

[1] Li J, Ding W and Fritz J S 2000 Separation of anions by ion chromatography-capillary electrophoresis *J. Chromatogr. A* **879** 245-57

[2] Kawamata T, Yamada M, Yasuda M and Seki M 2008 Continuous and precise particle separation by electroosmotic flow control in microfluidic devices *Electrophoresis* **29** 1423-30

[3] Wang X, Cheng C, Wang S and Liu S 2009 Electroosmotic pumps and their applications in microfluidic systems *Microfluid. Nanofluid.* **6** 145-62

[4] Gao M and Gui L 2014 A handy liquid metal based electroosmotic flow pump *Lab Chip* **14** 1866-72

[5] Lim C Y, Lam Y C and Yang C 2010 Mixing enhancement in microfluidic channel with a constriction under periodic electro-osmotic flow *Biomicrofluidics* **4** 014101

[6] Chang C C and Yang R J 2007 Electrokinetic mixing in microfluidic systems *Microfluid. Nanofluid.* **3** 501-25

[7] Wong P K, Chen C Y, Wang T H and Ho C M 2004 Electrokinetic bioprocessor for concentrating cells and molecules *Anal. Chem.* **76** 6908-14

[8] Hua Y, Jemere A B, Dragoljic J and Harrison D J 2013 Multiplexed electrokinetic sample fractionation, preconcentration and elution for proteomics *Lab Chip* **13** 2651-9

[9] Viovy J L 2000 Electrophoresis of DNA and other polyelectrolytes: Physical mechanisms *Rev. Mod. Phys.* **72** 813-72

[10] Horvath J and Dolnik V 2001 Polymer wall coatings for capillary electrophoresis *Electrophoresis* **22** 644-55
[11] Preisler J and Yeung E S 1996 Characterization of nonbonded poly (ethylene oxide) coating for capillary electrophoresis via continuous monitoring of electroosmotic flow *Anal. Chem.* **68** 2885-9
[12] Li W, Tegenfeldt J O, Chen L, Austin R H, Chou S Y, Kohl P A, Krotine J and Sturm J C 2003 Sacrificial polymers for nanofluidic channels in biological applications *Nanotechnology* **14** 578-83
[13] Kaji N, Tezuka Y, Takamura Y, Ueda M, Nishimoto T, Nakanishi H, Horiike Y and Baba Y 2004 Separation of long DNA molecules by quartz nanopillar chips under a direct current electric field *Anal. Chem.* **76** 15-22
[14] Miyazaki M, Kaneno J, Kohama R, Uehara M, Kanno K, Fujii M, Shimizu H and Maeda H 2004 Preparation of functionalized nanostructures on microchannel surface and their use for enzyme microreactors *Chem. Eng. J.* **101** 277-84
[15] Kusakabe K, Morooka S and Maeda H 2001 Development of a Microchannel Catalytic Reactor System *Korean J. Chem. Eng.* **18** 271-6
[16] Li D, Wu G S, Wang W, Wang Y D, Liu D, Zhang D C, Chen Y F, Peterson G P and Yang R 2012 Enhancing flow boiling heat transfer in microchannels for thermal management with monolithically-integrated silicon nanowires *Nano Lett.* **12** 3385-90
[17] Nagayama G, Sibuya S, Kawagoe M and Tsuruta T 2007 Heat transfer enhancement at nanostructured surface in parallel-plate microchannel. In: *Challenges on Power Engineering and Environment - Proceedings of the International Conference on Power Engineering 2007, ICOPE 2007,*
[18] Ng E, Chen K, Hang A, Syed A and Zhang J X J 2016 Multi-Dimensional Nanostructures for Microfluidic Screening of Biomarkers: From Molecular Separation to Cancer Cell Detection *Ann. Biomed. Eng.* **44** 847-62
[19] Li X, Yin H and Que L 2013 A microfluidic nanostructured fluorescence sensor for biomolecular binding detection. In: *Proceedings of IEEE Sensors,*
[20] Yasui T, Kaji N, Mohamadi M R, Okamoto Y, Tokeshi M, Horiike Y and Baba Y 2011 Electroosmotic flow in microchannels with nanostructures *ACS Nano* **5** 7775-80
[21] Koga Y, Kuriyama R, Sato Y, Hishida K and Miki N 2013 Effects of micromachining processes on electro-osmotic flow mobility of glass surfaces *Micromachines* **4** 67-79
[22] Kang S and Suh Y K 2009 Numerical analysis on electroosmotic flows in a microchannel with rectangle-waved surface roughness using the Poisson–Nernst–Planck model *Microfluid. Nanofluid.* **6** 461-77
[23] Messinger R J and Squires T M 2010 Suppression of electro-osmotic flow by surface roughness *Phys. Rev. Lett.* **105** 144503
[24] Fedder G K, Howe R T, Liu T J K and Quévy E P 2008 Technologies for cofabricating MEMS and electronics *Proc. IEEE* **96** 306-22
[25] Friedrich C R, Coane P J and Vasile M J 1997 Micromilling development and applications for microfabrication *Microelectron. Eng.* **35** 367-72
[26] Kummrow A, Theisen J, Frankowski M, Tuchscheerer A, Yildirim H, Brattke K, Schmidt M and Neukammer J 2009 Microfluidic structures for flow cytometric analysis of hydrodynamically focussed blood cells fabricated by ultraprecision micromachining *Lab Chip* **9** 972-81
[27] Waddell E A, Locascio L E and Kramer G W 2002 UV laser micromachining of polymers for microfluidic applications *J. Lab. Autom.* **7** 78-82
[28] Rossier J S, Schwarz A, Reymond F, Ferrigno R, Bianchi F and Girault H H 1999 Microchannel networks for electrophoretic separations *Electrophoresis* **20** 727-31
[29] Abdelgawad M, Watson M W L, Young E W K, Mudrik J M, Ungrin M D and Wheeler A R 2008 Soft lithography: Masters on demand *Lab Chip* **8** 1379-85
[30] Duffy D C, McDonald J C, Schueller O J and Whitesides G M 1998 Rapid prototyping of microfluidic systems in poly (dimethylsiloxane) *Anal. Chem.* **70** 4974-84
[31] Guckenberger D J, Jr., De Groot T E, Wan A M D, Beebe D J and Young E W K 2015 Micromilling: A method for ultra-rapid prototyping of plastic microfluidic devices *Lab Chip* **15** 2364-78
[32] Tanvir Ahmmed K M, Grambow C and Kietzig A M 2014 Fabrication of micro/nano structures on metals by femtosecond laser micromachining *Micromachines* **5** 1219-53
[33] McDonald J C, Duffy D C, Anderson J R, Chiu D T, Wu H, Schueller O J A and Whitesides G M 2000 Fabrication of microfluidic systems in poly(dimethylsiloxane) *Electrophoresis* **21** 27-40
[34] McDonald J C and Whitesides G M 2002 Poly (dimethylsiloxane) as a material for fabricating microfluidic devices *Acc. Chem. Res.* **35** 491-9

[35] Koo N, Bender M, Plachetka U, Fuchs A, Wahlbrink T, Bolten J and Kurz H 2007 Improved mold fabrication for the definition of high quality nanopatterns by Soft UV-Nanoimprint lithography using diluted PDMS material *Microelectron. Eng.* **84** 904-8
[36] Kang H, Lee J, Park J and Lee H H 2005 An improved method of preparing composite poly (dimethylsiloxane) moulds *Nanotechnology* **17** 197
[37] Con C and Cui B 2013 Effect of mold treatment by solvent on PDMS molding into nanoholes *Nanoscale Res. Lett.* **8** 1-6
[38] Archer M J and Ligler F S 2008 Fabrication and characterization of silicon micro-funnels and tapered micro-channels for stochastic sensing applications *Sensors* **8** 3848-72
[39] Schlautmann S, Besselink G A J, Prabhu G R and Schasfoort R B M 2003 Fabrication of a microfluidic chip by UV bonding at room temperature for integration of temperature-sensitive layers *J. Micromech. Microeng.* **13** S81-S4
[40] Heyderman L J, Schift H, David C, Gobrecht J and Schweizer T 2000 Flow behaviour of thin polymer films used for hot embossing lithography *Microelectron. Eng.* **54** 229-45
[41] Ting C J, Huang M C, Tsai H Y, Chou C P and Fu C C 2008 Low cost fabrication of the large-area anti-reflection films from polymer by nanoimprint/hot-embossing technology *Nanotechnology* **19**
[42] Jena R K, Yue C Y, Lam Y C, Tang P S and Gupta A 2012 Comparison of different molds (epoxy, polymer and silicon) for microfabrication by hot embossing technique *Sens. Actuators B Chem.* **163** 233-41
[43] Benitez-Rangel J P, Domínguez-González A, Herrera-Ruiz G and Delgado-Rosas M 2007 Filling process in injection mold: A review *Polym. Plast. Technol. Eng.* **46** 721-7
[44] Utko P, Persson F, Kristensen A and Larsen N B 2011 Injection molded nanofluidic chips: Fabrication method and functional tests using single-molecule DNA experiments *Lab Chip* **11** 303-8
[45] Nguyen Q M P, Chen X, Lam Y C and Yue C Y 2011 Effects of polymer melt compressibility on mold filling in micro-injection molding *J. Micromech. Microeng.* **21**
[46] Andresen K Ø, Hansen M, Matschuk M, Jepsen S T, Sørensen H S, Utko P, Selmeczi D, Hansen T S, Larsen N B, Rozlosnik N and Taboryski R 2010 Injection molded chips with integrated conducting polymer electrodes for electroporation of cells *J. Micromech. Microeng.* **20**
[47] Tanzi S, Ostergaard P F, Matteucci M, Christiansen T L, Cech J, Marie R and Taboryski R 2012 Fabrication of combined-scale nano- and microfluidic polymer systems using a multilevel dry etching, electroplating and molding process *J. Micromech. Microeng.* **22**
[48] Piotter V, Hanemann T, Ruprecht R and Haußelt J 1997 Injection molding and related techniques for fabrication of microstructures *Microsys. Technol.* **3** 129-33
[49] Kupka R K, Bouamrane F, Cremers C and Megtert S 2000 Microfabrication: LIGA-X and applications *Appl. Sci. Res.* **164** 97-110
[50] Elders J, Jansen H V, Elwenspoek M and Ehrfeld W 1995 DEEMO: a new technology for the fabrication of microstructures. In: *Proc. IEEE MEMS '95,* pp 238-43
[51] Burn Jeng L 1975 Deep UV lithography *J. Vac. Sci. Technol.* **12** 1317-20
[52] Kawamura Y, Toyoda K and Namba S 1982 Deep uv submicron lithography by using a pulsed high-power excimer laser *J. Appl. Phys.* **53** 6489-90
[53] Liu K, Avouris P, Bucchignano J, Martel R, Sun S and Michl J 2002 Simple fabrication scheme for sub-10 nm electrode gaps using electron-beam lithography *Appl. Phys. Lett.* **80** 865-7
[54] Grigorescu A E and Hagen C W 2009 Resists for sub-20-nm electron beam lithography with a focus on HSQ: state of the art *Nanotechnology* **20** 292001
[55] Chang H C and Yeo L Y 2010 *Electrokinetically Driven Microfluidics and Nanofluidics: Chapter 3: Electro-Osmotic Transport* (New York: Cambridge University Press)
[56] Kirby B J 2010 *Micro- and Nanoscale Fluid Mechanics: Transport in Microfluidic Devices: Chapter 6: Electroosmosis* (New York: Cambridge University Press)
[57] Persson F and Tegenfeldt J O 2010 DNA in nanochannels—directly visualizing genomic information *Chem. Soc. Rev.* **39** 985-99
[58] Koh C G, Tan W, Zhao M-q, Ricco A J and Fan Z H 2003 Integrating polymerase chain reaction, valving, and electrophoresis in a plastic device for bacterial detection *Anal. Chem.* **75** 4591-8
[59] Huang X, Gordon M J and Zare R N 1988 Current-monitoring method for measuring the electroosmotic flow-rate in capillary zone electrophoresis *Anal. Chem.* **60** 1837-8
[60] Ren L, Escobedo C and Li D 2002 A new method of evaluating the average electro-osmotic velocity in microchannels *J. Colloid Interface Sci.* **250** 238-42

[61] Ren L, Masliyah J and Li D 2003 Experimental and theoretical study of the displacement process between two electrolyte solutions in a microchannel *J. Colloid Interface Sci.* **257** 85-92
[62] Pittman J L, Henry C S and Gilman S D 2003 Experimental studies of electroosmotic flow dynamics in microfabricated devices during current monitoring experiments *Anal. Chem.* **75** 361-70
[63] Lim A E, Lim C Y and Lam Y C 2015 Electroosmotic flow hysteresis for dissimilar ionic solutions *Biomicrofluidics* **9** 024113
[64] Lim A E, Lim C Y and Lam Y C 2016 Electroosmotic flow hysteresis for dissimilar anionic solutions *Anal. Chem.* **88** 8064-73
[65] Lim C Y and Lam Y C 2012 Direction dependence of displacement time for two-fluid electroosmotic flow *Biomicrofluidics* **6** 012816
[66] Lim C Y, Lim A E and Lam Y C 2016 Ionic Origin of Electro-osmotic Flow Hysteresis *Sci. Rep.* **6** 22329
[67] Rodríguez I and Chandrasekhar N 2005 Experimental study and numerical estimation of current changes in electroosmotically pumped microfluidic devices *Electrophoresis* **26** 1114-21
[68] Yan D G, Yang C and Huang X Y 2007 Effect of finite reservoir size on electroosmotic flow in microchannels *Microfluid. Nanofluid.* **3** 333-40
[69] Corstjens H, Billiet H A H, Frank J and Luyben K C A M 1996 Variation of the pH of the background electrolyte due to electrode reactions in capillary electrophoresis: Theoretical approach and in situ measurement *Electrophoresis* **17** 137-43
[70] Tang G, Yan D, Yang C, Gong H, Chai J C and Lam Y C 2006 Assessment of Joule heating and its effects on electroosmotic flow and eletrophoretic transport of solutes in microfluidic channels *Electrophoresis* **27** 628-39
[71] Arulanandam S and Li D 2000 Determining ζ potential and surface conductance by monitoring the current in electro-osmotic flow *J. Colloid Interface Sci.* **225** 421-8

Supplementary Data

Effect of nanostructures orientation on electroosmotic flow in a microfluidic channel

An Eng Lim[1], Chun Yee Lim[1], Yee Cheong Lam[1,4], Rafael Taboryski[2], and Shu Rui Wang[3]

[1]*School of Mechanical and Aerospace engineering, Nanyang Technological University, 50 Nanyang Avenue, Singapore 639798*

[2]*Department of Micro- and Nanotechnology, Technical University of Denmark, 2800 Kongens Lyngby, Denmark*

[3]*Park Systems Pte Ltd, #01-07 The Alpha, Science Park 2, Singapore 117684*

E-mail: myclam@ntu.edu.sg

[4]Author to whom any correspondence should be addressed.

Fabrication of smooth microchannel

The smooth microchannel was fabricated via the conventional DEEMO (**D**ry **E**tching, **E**lectroplating, **MO**lding) process as shown in figure S1, and the detailed process parameters are presented in table S1.

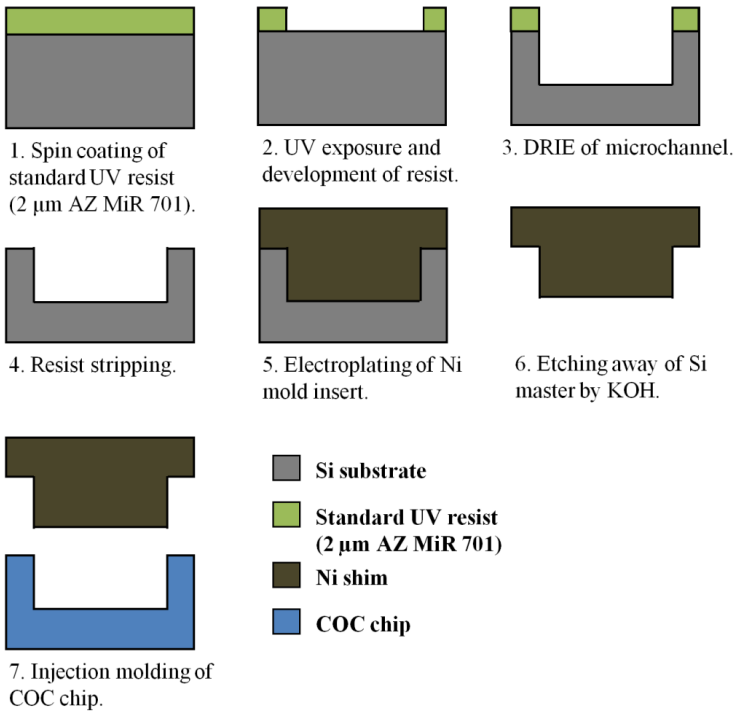

Figure S1. Schematics of DEEMO fabrication process for smooth microchannel.

Table S1. Process parameters of DEEMO fabrication process for smooth microchannel.

Process	Parameters for smooth microchannel
Spin coating of photoresist on Si	HMDS priming. 2 µm AZ MiR 701 positive resist, spin-off 30 s at 2600 rpm. Prebaking: 90 °C for 1 min.
Photolithography	350 W Hg lamp with i-line filter as light source, 365 nm wavelength. W/A = 7 mW/cm^2; t = 25 s. Post exposure bake: 110 °C for 1 min, then puddled in TMAH developer for 1 min.
Deep reactive ion etching (DRIE)	Passivation>>Etch: C_4F_8>>SF_6/O_2 = 150>>275/15 sccm; Coil/Platen power = 2000/0>>2500/35 W; Pressure = 20>>26 mtorr; t = 1>>2.2 s; Cycles = 75; Temperature = 0 °C.

Resist stripping	O_2/N_2 = 400/70 sccm; Pressure = 1 mbar; Power = 1000 W; t = 10 min.
Electroplating	Sputtering of 85 nm Ni/V seed layer (93/7 wt%). Electroplating Ni shim of 350 µm thickness: Maximum current = 3.5 A; Charge = 18.1 Ah; t = 6 h.
KOH etching	25 wt% KOH: Temperature = 80 °C; t = 8 h.
Injection molding	Mold temperature = 90 °C; Melt temperature = 270 °C; Injection pressure = 950 ± 25 bar; Injection velocity = 37 mm/s; Holding pressure = 600 ± 25 bar for 3 s; cooling time = 30 s; Pre-drying (Permanent) = 90 °C; Cycle time = 30 s to 1 min.